A Vanadium Redox Flow Process for Carbon Capture and Energy Storage

Mohsen Afshari[1], Abdelrahman Refaie[1], Prince Aleta[1], Ahmad Hassan[1], Mim Rahimi[1,2,*]

[1] Department of Civil and Environmental Engineering, University of Houston, Houston, TX 77204, USA
[2] Materials Science and Engineering Program, University of Houston, Houston, TX 77204, USA
* Corresponding Author: mrahimi@uh.edu

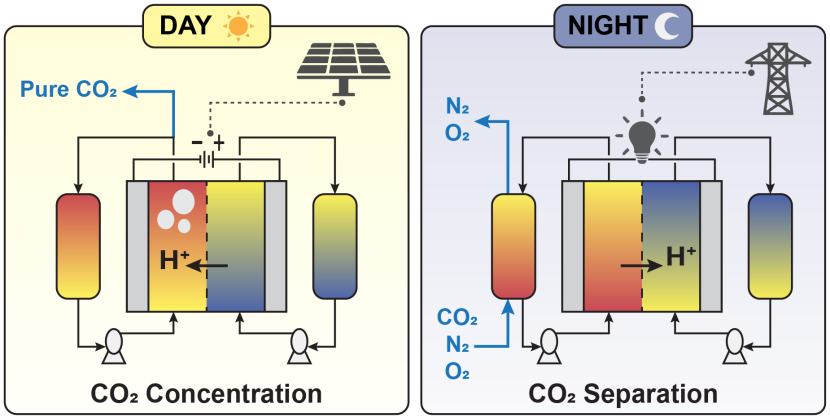

ABSTRACT

Climate change mitigation by decreasing worldwide CO_2 emissions is an urgent and demanding challenge that requires innovative technical solutions. This work, inspired by vanadium redox flow batteries (VRFB), introduces an integrated electrochemical process for carbon capture and energy storage. It utilizes established vanadium and ferricyanide redox couples for pH modulation for CO_2 desorption and absorbent regeneration. The developed process consumes electricity during the daytime—when renewable electricity is available—to desorb CO_2 and charge the cell, and it can regenerate the absorbent for further CO_2 absorption while releasing electricity to the grid during nighttime when solar power is unavailable. This research explores the process fundamentals and scalability potential, through an extensive study of the system's thermodynamics, transport phenomena, kinetics, and bench-scale operations. Cyclic voltammetry (CV) was utilized to study the thermodynamics of the process, mapping the redox profiles to identify ideal potential windows for operation. The CV results pinpointed a 0.3 V Nernstian overpotential as the thermodynamic minimum required for cell operation. Additionally, polarization studies were conducted to select the practical operating potential, identifying 0.5 V as optimal for the CO_2 desorption cycle to provide sufficient polarity to overcome activation barriers in addition to the Nernstian potential. Mass transfer analysis balanced conductivity and desorption efficiency, with a 1:1 ratio identified as optimal for redox-active species and background electrolyte concentration. To further enhance the kinetics of the redox reactions, plasma treatment of electrode surfaces was implemented, resulting in a 43% decrease in charge transfer resistance, as measured by electrochemical impedance spectroscopy (EIS) analysis. Finally, a bench-scale operation of the system demonstrated an energy consumption of 54 kJ/mol CO_2, which is competitive with other electrochemical carbon capture technologies. Besides its energy competitiveness, the process offers multiple additional advantages, including the elimination of precious metal electrodes, oxygen insensitivity in flue gas, scalability inspired by VRFB technology, and the unique ability to function as a battery during the absorbent regeneration process, enabling efficient day-night operation.

Keywords: Climate Change; Carbon Capture; Electrochemistry; VRFB; Energy Storage

1. INTRODUCTION

Human activity is significantly affecting the Earth's climate, resulting in 1.18°C rise in global temperature since pre-industrial periods, primarily caused by carbon dioxide (CO_2) emissions [1]. The Intergovernmental Panel on Climate Change (IPCC) emphasizes the necessity of limiting global warming within the range of 1.5°C to 2.0°C in order to avoid irreversible consequences [2]. The current annual global CO_2 emissions exceed 36 gigatons, and if they continue to increase, reaching the climate goals will be impossible [3–6]. Several technological solutions are being investigated to reduce the global CO_2 emissions, such as decarbonization technologies that aim to decrease the emissions by transitioning to renewable energy sources and enhancing energy efficiency [4]. Carbon capture and storage (CCS) is a promising technology that captures CO_2 from point sources, such as power plants and industrial facilities, followed by sequestration [7]. Although CCS has the potential for global-scale deployment, its actual implementation has been slower than expected [7,8]. However, it continues to be a crucial part of the plan to reduce the impact of climate change and meet emission reduction goals [5]. This highlights the significance of ongoing research, development, and implementation of CCS to tackle global carbon emissions.

Various technologies have been developed for a wide range of CCS applications. Among these, the sorption-based method, often utilizing an amine absorbent, has received the most attention [9–11]. This two-step process involves an amine scrubbing tower followed by a thermally driven amine regeneration step. However, challenges persist with sorption-based processes. The regeneration step, which employs thermal swing, necessitates a significant energy requirement [7,12–14]. Furthermore, operating at elevated temperatures during this step significantly accelerates the thermal degradation of the amine absorbent. The research community is actively addressing these issues by developing alternative amines that require lower desorption temperatures and exhibit greater thermal stability over a wider temperature range.

Electrochemical carbon capture (ECC) processes have recently emerged as an alternative approach to the thermally driven absorbent methods [4,15–17]. ECCs rely on redox reactions to desorb CO_2 through an electro-swing mechanism. Due to this unique desorption mechanism, ECCs offer several advantages, including lower energy requirements, eliminating the need to operate at elevated temperatures, and minimizing the rate of absorbent degradation [4,5,15,18]. Additionally, ECCs offer the inherent advantages of electrochemical systems, such as modularity, scalability, and ease of retrofitting [4]. ECC technologies are still in the early stages of development, with the primary research focus on addressing issues related to selectivity, stability, and efficiency. Additionally, the energy requirements for CO_2 capture remain a central focus of research, and a broad range of strategies is being investigated to further reduce these energy demands [4].

Several ECC approaches have been developed, including the electrochemical generation of nucleophiles (EGN) [19–24], electrochemical capacitive adsorption (ECA) [25–30], electrochemically mediated amine regeneration (EMAR) [31–36], and electrochemical modulation of proton concentration (EMPC), also known as electrochemical pH swing [37–43]. These approaches differ in how they utilize redox reactions to capture and concentrate CO_2. For instance, EGNs rely on the generation of nucleophilic sites on a redox-active molecule (e.g., quinone, Q) via reduction to initiate the selective capture of CO_2 from its electrophilic carbon site.

On the anode, the Q-CO_2 adduct is oxidized, resulting in the regeneration of the redox-active molecule and the separation and concentration of CO_2. In contrast, EMAR involves a metal redox reaction (e.g., copper) to facilitate the desorption of CO_2 captured by an amine absorbent; therefore, the redox reaction mediates the desorption processes, as opposed to the EGN approach, which the redox reaction is directly involved.

ECCs based on EMPC, or pH swing, leverage the pH sensitivity of the CO_2 equilibrium, whereby CO_2 is absorbed as bicarbonate and carbonate species at high pH values and desorbed at lower pH values as gaseous CO_2 [44]. Electrochemically-driven pH swing processes establish the necessary pH conditions for absorption (high pH) and desorption (low pH) through a proton-coupled electron transfer (PCET) redox reaction. Several pH swing processes have been developed, each with its own unique approach and challenges. Membrane electrodialysis (MED) systems employ a series of ion-exchange and water-dissociating bipolar membranes, which facilitate CO_2 capture and release through the generation of hydroxide and protons, respectively [39,40,42,45–48]. Another method, the redox-mediated pH swing process, utilizes quinone compounds that can reversibly couple with proton during reduction or oxidation to modulate the solution pH, i.e., $Q + n\,H^+ + n\,e^- \rightleftharpoons QH_n$ [43,49–53]. In this process, CO_2 is captured as HCO_3^- in the cathode compartment, where quinone reduction consumes proton, increasing the local pH. The HCO_3^- ions subsequently move towards the anode through the electromigration and diffusion mechanisms. At the anode, the process of quinone oxidation occurs, which leads to the release of protons. This causes a decrease in the local pH and facilitates the release of CO_2. A third approach, the proton concentration process (PCP), utilizes proton-intercalating electrode materials, such as manganese dioxide [54,55]. The PCP process comprises two stages: chemical absorption of CO_2 using potassium carbonate and electrochemical desorption. The CO_2-rich stream from the absorber is directed to the anode compartment, where proton deintercalation from the electrode increases the proton concentration, driving the equilibrium towards the release of CO_2 in gaseous form. Subsequently, the CO_2-lean stream is directed to the cathode compartment, where the alkalinity of the absorbent is regenerated via proton intercalation on the cathode.

While these pH swing systems show promise, they also face challenges that hinder their widespread adoption. MED systems are associated with high costs due to the need for multiple membranes and the energy-intensive water splitting reaction, which additionally requires costly catalysts [4,48]. Redox-mediated pH swing processes face challenges such as the complexity of incorporating precious metal catalysts, the low solubility of the active components [4], and the sensitivity to oxygen impurities [56,57]. Recent investigations on redox-mediated pH swing systems have focused on improving the solubility of the active compound [53] and mitigating oxygen sensitivity [57,58]. PCP systems, while not constrained by solubility limitations, require the development of electrodes with enhanced stabilities and proton capacities [4].

In this study, a novel electrochemically-driven pH swing process has been developed to effectively address the challenges associated with previous systems. The new system was inspired by the well-known vanadium redox flow batteries (VRFB) and integrates CO_2 chemistry. In one chamber, a vanadium PCET redox reaction generates proton ions. These protons are then transferred to the other chamber through a proton exchange membrane (PEM), facilitating the desorption of CO_2. Therefore, the chamber containing the PCET compound, and the chamber involved in CO_2

chemistry are decoupled, with the membrane between the two chambers functioning as a proton pump.

This system offers several advantages. First, by decoupling the chamber involving the PCET reaction from the chamber with electrolyte exposed to flue gas, the negative impact of impurities in the gas phases, especially O_2, is effectively mitigated. In previous systems, the redox-active compound responsible for the pH swing was present in the same chamber as the gas phase. Second, the proton pump interface helps address potential issues related to Nernstian overpotentials caused by proton accumulation, as the generated ions are actively transferred through the proton pump. Lastly, as the system is inspired by the well-established VRFB technology, the solubility of the active compound is significantly high, and it also inherently possesses the capability to store and harvest energy as needed.

The proposed process integrates the principles of flow batteries with absorbent-based CO_2 separation. The system comprises an absorption column and a two-chamber electrochemical cell, (Figure 1). The posolyte (positive electrolyte) and the negolyte (negative electrolyte) chambers of the electrochemical cell are separated by a PEM. The posolyte contains a vanadium redox couple (VO^{2+}/VO_2^{+}), while the negolyte comprises a ferricyanide/ferrocyanide redox couple ($Fe(CN)_6^{3-}/Fe(CN)_6^{4-}$). In the absorption column, CO_2 is captured using a potassium carbonate (K_2CO_3) solution as the absorbent. The CO_2-rich solution, containing dissolved CO_2 in the form of HCO_3^- and CO_3^{2-} ions, is then directed to the negolyte chamber of the electrochemical cell. During the desorption cycle (Figure 1A), a potential is applied to the cell, initiating the oxidation of VO^{2+} to VO_2^{+} (i.e., $VO^{2+} + H_2O \rightarrow VO_2^{+} + 2H^{+} + e^{-}$) in the posolyte, generating protons that migrate through the PEM into the negolyte. The influx of protons lowers the negolyte's pH, shifting the carbonate equilibrium towards the formation of dissolved CO_2, releasing the absorbed CO_2 from the solution. Simultaneously, $Fe(CN)_6^{3-}$ is reduced to $Fe(CN)_6^{4-}$ in the negolyte, maintaining charge balance. As evidenced by an increase in the open circuit potential (OCP) of the cell during the desorption cycle, the system shows the ability to store electricity similar to the charge cycle of the redox flow batteries, which the stored electricity can be released in the reverse cycle. After the desorption cycle, when the current drops below the set threshold, to regenerate the VO^{2+} and $Fe(CN)_6^{3-}$ ions, the polarization is reversed, leading to the reduction of VO_2^{+} back to VO^{2+} in the posolyte. This requires consumption of protons through the PCET reaction; therefore, it facilitates the withdrawal of protons from the negolyte to the posolyte. This increases the negolyte's pH, enhancing its capacity to absorb CO_2 in the subsequent absorption cycle. Meanwhile, $Fe(CN)_6^{4-}$ is oxidized back to $Fe(CN)_6^{3-}$ in the negolyte, completing the redox cycle. The choice of the $Fe(CN)_6^{3-}/Fe(CN)_6^{4-}$ redox couple in the negolyte is an important aspect of this process due to its stability and effectiveness in aqueous redox flow batteries [59], and compatibility with the optimal pH range for CO_2 absorption and desorption (between pH of 4 and 10). In contrast, the V^{3+}/V^{2+} redox couple, commonly used in all-vanadium redox flow batteries, tends to precipitate in this pH range, making it less practical for this process. Additionally, the $Fe(CN)_6^{3-}/Fe(CN)_6^{4-}$ redox reaction is not a PCET reaction. This ensures that the redox reaction in the negolyte does not consume the transferred proton ions to this chamber, which are required to desorb CO_2 via the pH swing mechanism.

In an ideal operation, the proposed system can be integrated with renewable energy sources like solar power, enabling it to operate in a day-night cycle. During the day, the system can utilize the

available electricity to drive the CO_2 desorption process, simultaneously storing the excess energy in the form of chemical potential within the electrolytes. At night, the stored energy can be discharged, providing electricity to the grid while simultaneously driving the CO_2 absorption process. This day-night operation allows the system to contribute to the grid balance by storing and delivering electrical energy as needed, making it a promising solution for the integration of renewable energy sources and carbon capture technologies. In particular, with the rising interest in the local smaller-scale electricity grid for industrial plants, this process has the potential to integrate the point source carbon capture into these local power systems.

This article presents proof of concept of the proposed ECC, focusing on the fundamental understandings of the process thermodynamics, kinetics, and mass transport phenomena as well as electrolyte chemistry. Furthermore, the bench-scale operation of the system is demonstrated along with the reversibility over multiple cycles. Ultimately, the energetics, efficiency, and potential for energy storage are discussed and compared with other ECC technologies, offering a comprehensive overview of the developed system's capabilities.

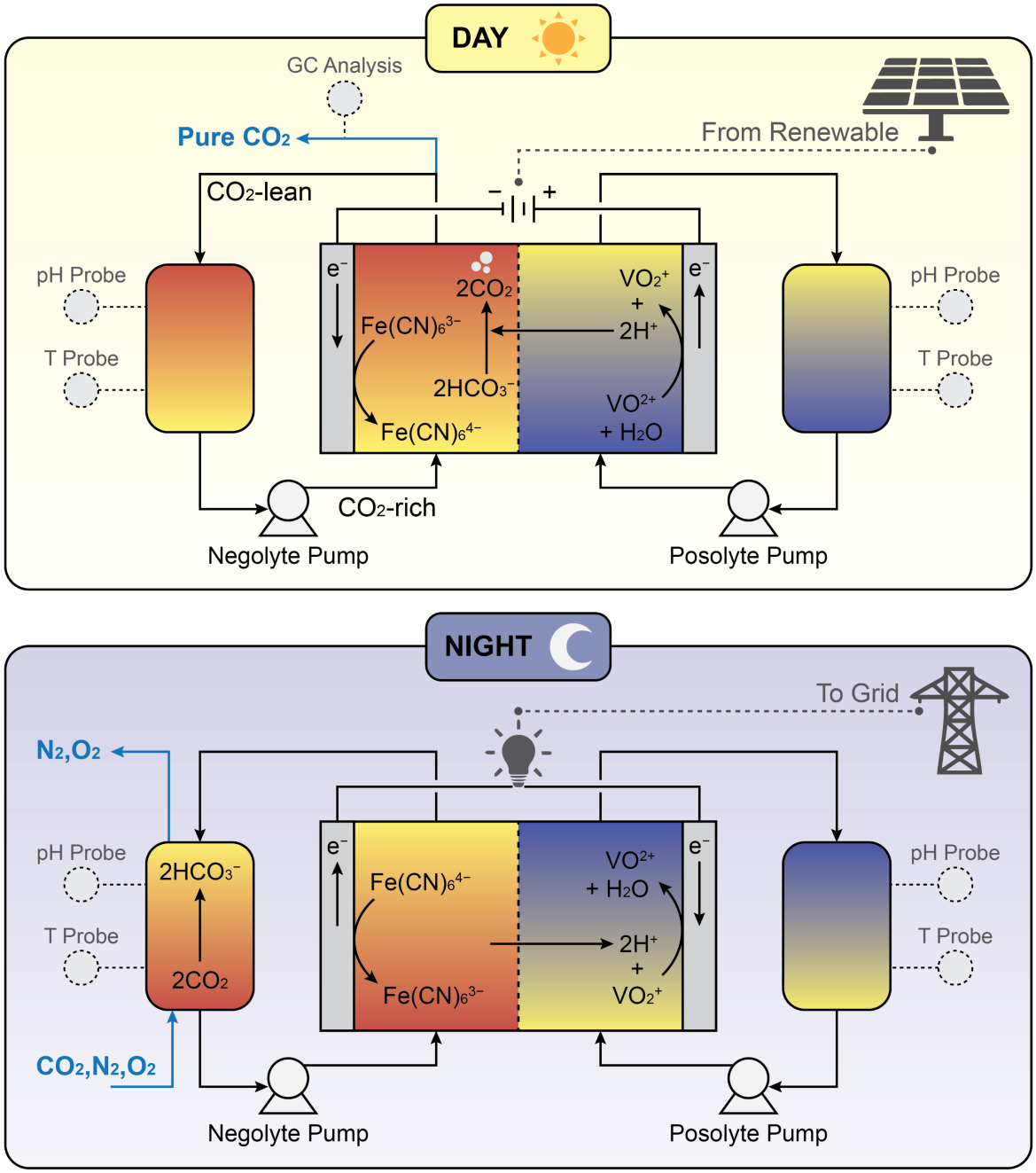

Figure 1. A schematic of the process during the day and night cycles. The figure shows the proposed operation of the system during the day and night times. In the day cycle when the solar energy is available, the process consumes electricity, resulting in the generation of protons in the posolyte and transport of them to the negolyte chamber, shifting the bicarbonate equilibrium towards gaseous CO_2. Simultaneously, energy is stored in the cell with the increase in the open circuit voltage (OCP). During the night cycle, the absorbent is regenerated with the increase in the negolyte pH as a result of the transport of protons from the negolyte to the posolyte chamber. Simultaneously, the VO_2^+ and $Fe(CN)_6^{4-}$ species that were produced during the day cycle are reduced and oxidized back to their initial states, respectively. In this step, the stored electrical energy during the desorption cycle is released to the grid.

2. MATERIALS AND METHODS

2.1. Electrolytes Preparation

The chemical solutions for the study were prepared using deionized water with a resistivity exceeding 18 MΩ·cm, ensuring an ultra-pure medium. The vanadium (IV) oxide sulfate hydrate ($VOSO_4.xH_2O$; 97% purity, Sigma Aldrich) was used to prepare the posolyte solutions, providing a source of vanadyl ionic species (VO^{2+}). Similarly, potassium hexacyanoferrate (III) ($K_3Fe(CN)_6$; 99.0% purity, Sigma Aldrich) was dissolved in the negolyte solutions, introducing ferricyanide ionic species ($Fe(CN)_6^{3-}$) as the redox active species for the cathodic reactions. To improve the conductivity and overall electrochemical performance of the solutions, potassium sulfate (K_2SO_4; purity >99.0%, Sigma Aldrich) was added as a background electrolyte to each sample. Potassium carbonate (K_2CO_3; 99.0% purity, Sigma Aldrich) was used to increase the dissolved inorganic carbon (DIC) level of electrolyte, when needed, e.g., for the cyclic voltammetry (CV) studies. Additionally, potassium bicarbonate ($KHCO_3$; 99.7% purity, Sigma Aldrich) was dissolved in the negolyte solutions to simulate the conditions of a CO_2-rich stream, simulating the outlet from an absorption column.

2.2. Cell Design and Fabrication

To conduct the experiments, two cells were designed and fabricated. CV tests were carried out using a batch three-electrode cell, while a flow-based cell was developed for broader experiments specifically targeting CO_2 desorption and absorbent regeneration cycles in the bench scale operation. The CV cell employed a conventional three-electrode setup, consisting of a glassy carbon electrode as the working electrode (WE; BASi), a platinum wire as the counter electrode (CE; 99.9% purity, Sigma Aldrich), and an Ag/AgCl electrode as the reference electrode (RE; saturated KCl; ALS). The electrodes were positioned with precision, maintaining a distance of 2.5 cm between them to ensure measurement consistency.

The flow cell was specifically designed for more complex experiments, incorporating cathode and anode made from solid graphite plates–an electrode material that has been commonly used in VRFBs and other energy storage systems [60–63]. These were divided by a PEM (Nafion N-117). The design included flow channels within each electrode, resulting in a specific surface area of 5 cm^2. The electrodes were of equal dimensions and positioned at a distance of 0.2 cm from each other. Two solid copper plates were used as current collectors for the graphite electrodes and were reinforced by endplates made of high-density polyethylene (HDPE), measuring 9.3 x 9.3 cm. This configuration facilitated the regulated flow of posolyte and negolyte solutions between their respective compartments and external storage containers, circulated by a peristaltic pump (Reglo Peristaltic Pump; Ismatec) with four separate and adjustable channels (Figure 2). The negolyte's pH was also monitored using a precision pH meter (APERA Instruments; pH800). This design allowed for the precise study of electrochemical processes and served as a representation of a bench-scale operation.

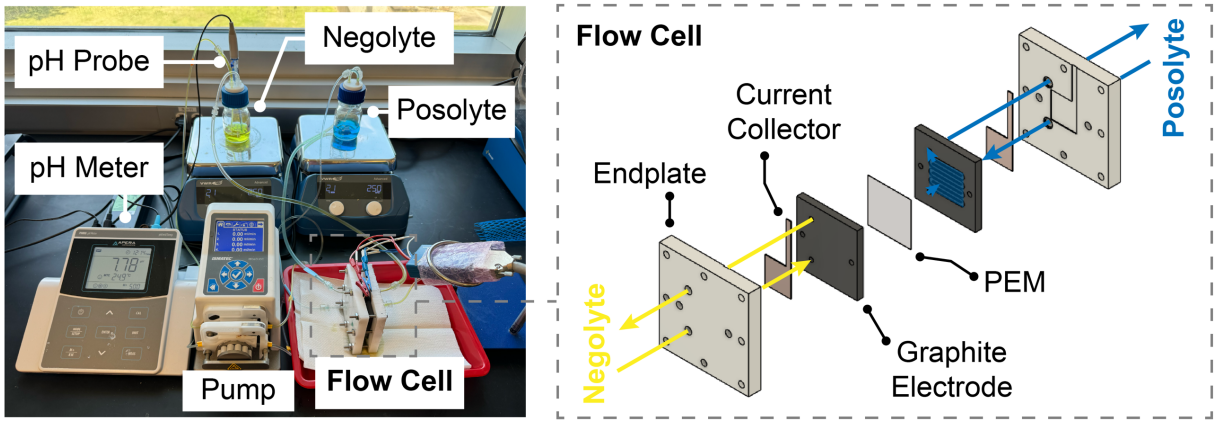

Figure 2. An Illustration of the experimental setup. The left panel displays the components of the developed process, including the flow cell, posolyte and negolyte tanks, a pH monitoring system, and a multichannel pump to circulate the electrolytes between the tanks and the cell. The right panel provides a detailed zoom-in view of the flow cell, including the endplate, current collector, graphite electrodes, and proton exchange membrane (PEM).

2.3. Electrode Plasma Treatment

To investigate the influence of electrode surface characteristics on redox reactions, plasma treatment of graphite electrodes with atmospheric air was selected as a method to explore potential enhancements in the performance. A plasma cleaner (HARRICK PLASMA; PDC-32G) was used to treat both the cathode and anode for 10 minutes, applying 11 W to the radio frequency coil. The change in the contact angle of the graphite electrodes when exposed to a water droplet was measured before and after the plasma treatment. A compact high-resolution CMOS camera (THORLABS; DCC1645C), a 12X zoom lens (THORLABS; MVL12X12Z), and a pipettor (Matrix Technologies; micro-Electrapette 25) dispensing liquids from a disposable pipette tip were used to measure the contact angle data. After completing the plasma treatment, to study its impact on the current density, chronoamperometry test was employed to apply a potential of 0.5 V to the cell, both pre- and post-plasma treatment, and the achieved current density was recorded. Additionally, the impact of plasma treatment was evaluated through the measurement of charge transfer resistance using electrochemical impedance spectroscopy (EIS).

2.4. Electrochemical Analysis

In this study, various electrochemical techniques were employed to examine the process's core behaviors, including CV, chronoamperometry (CA), and EIS. CV was crucial for identifying the distinct redox peaks of vanadium and ferricyanide to determine the desired reactions for the pH-swing, central to the process. CA was utilized in experiments involving constant potential application, such as the CO_2 desorption and absorbent regeneration experiments. EIS was used to evaluate resistance components, especially in studies of mass transfer and electrode treatment. All of the electrochemical characterizations were conducted using a multi-channel potentiostat (BioLogic; VMP-300), with data interpretation carried out through the built-in software

(BioLogic; EC-Lab), alongside Microsoft Excel and OriginLab for comprehensive data analysis and visualization.

Cyclic Voltammetry. In the vanadium CV tests, the potential of WE was adjusted from 0 V to 1 V relative to the RE. This was done at a relatively slow scan rate of 5 mV/s to cover all possible redox reactions at different potentials. For detailed analysis, the range of the potential sweep was further limited to 0.35 V to 0.8 V vs. RE. In ferricyanide CV studies, the effect of dissolved carbonate and bicarbonate on redox peaks was assessed by sweeping the potential from 0 V to 0.6 V versus RE and at the scan rate of 25 mV/s.

Chronoamperometry. CA was employed for all CO_2 desorption experiments, including polarization curve analysis for the desorption cycle and absorbent regeneration step. The cell potential during the polarization experiment was adjusted at different values (0.25, 0.5, 0.75, 1, 1.25 V), and an unpolarized mode (0 V) was also included. Each experiment continued until the current became relatively stable. For all other remaining experiments, such as the CO_2 desorption and absorbent regeneration cycles, the system's performance was examined by applying specific potentials of 0.5 V and −0.5 V, respectively.

Electrochemical Impedance Spectroscopy. In the EIS experiments, a potential of 0.5 V was applied to the cell to analyze resistance components during the CO_2 desorption cycle. Measurements ranged a frequency range from 100 kHz to 300 mHz, with a 10 mV sinusoidal amplitude. The data were fitted to a Randles circuit model, appropriate for such systems [33,35,64–66], differentiating between ohmic resistance (R_{ohmic}) and charge transfer resistance (R_{ct}). The data were also depicted in the Nyquist plots, illustrating the model's fit, helping in the interpretation of electrochemical impedance and the system's resistance components.

2.5. DIC Analysis

The gas phase analysis was conducted using an integrated titration and gas chromatography (GC) approach, utilizing a liquid electrolyte sample. Direct gas phase analysis was not performed to avoid potential uncertainties associated with gas phase measurements, such as leaks in a non-airtight system. To analyze the DIC of the liquid phase, samples were taken from the negolyte and then titrated using a standard solution of 4M HCl. The objective of this approach was to shift the CO_2 equilibrium completely towards the production of gaseous CO_2 and quantify it. The amount of CO_2 released during the titration was precisely measured using a U-tube manometer.

To verify that only CO_2 was released during the acid titration procedure, the gas present in the headspace of the sample vials was analyzed using GC (Agilent; 990 Micro GC) both before and after the titration. The first channel employs argon as the carrier gas and can detect gases such as oxygen and nitrogen. The second channel utilizes helium as the carrier gas and can detect gases like methane, ethane, propane, butane, CO_2, and water vapor. Figure 3 demonstrates the outcomes of the headspace study before and after the acid titration. It shows that the first channel consistently identified the presence of oxygen and nitrogen, both before and after the titration. The second channel recognized the presence of CO_2 in the headspace only after acid titration, as shown in Figure 3. The studies verified that only CO_2 was released after titration, which validates the method for measuring the amount of CO_2 in the liquid phase and demonstrates the reliability of this analytical approach in analyzing the process of CO_2 desorption in the system.

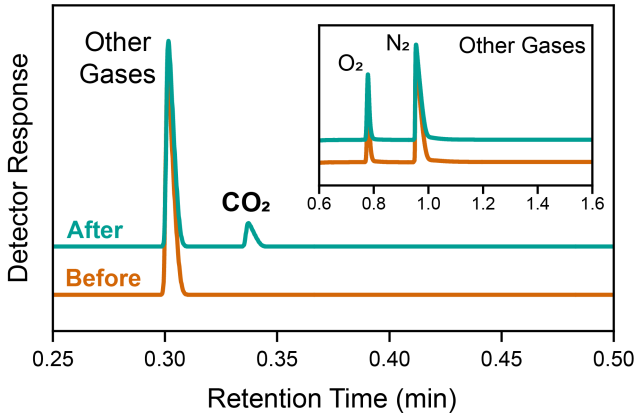

Figure 3. Gas chromatography analysis. The gas chromatography (GC) analysis of the gas desorbed by the acid titration method confirmed the successful desorption of only CO_2. Other gases, including O_2 and N_2, were consistently observed before and after the titration (inset); these originated from the air in the titration cell headspace, which contains O_2 and N_2. A two-channel GC was used to identify all the gas phase compounds.

2.6. Bench Scale Operation

In order to demonstrate a complete operational cycle of the process, a desorption experiment was conducted followed by a reverse cycle aimed at regenerating the redox-active species (VO^{2+} and $Fe(CN)_6^{3-}$) and restore the alkalinity for the following absorption step. The posolyte consisted of 0.25 molar $VOSO_4$ and K_2SO_4. The negolyte was intended to mimic a CO_2-enriched stream from an absorption column and consisted of 0.25 molar $K_3Fe(CN)_6$, K_2SO_4, and $KHCO_3$. CA was used to apply a constant potential of 0.5 V until approximately 70% of the initial VO^{2+} and $Fe(CN)_6^{3-}$ ions were utilized up. To regenerate the VO^{2+} and $Fe(CN)_6^{3-}$ species, the cell was subjected to reverse polarization at a potential of −0.5V until it reached a state of charge (SOC) of 20%. The negolyte's pH was also monitored using the pH meter. The process energetics and efficiency were then calculated. To evaluate the process' reversibility over multiple cycles, the cell was subjected to the polarization of 0.5 and −0.5 V, which represent the operation of the cell over day and night, respectively. Initially, a potential of 0.5 V was applied to the cell until 50% SOC was reached, and then the cell potential was changed to −0.5 V. The polarization was then switched for 10 full cycles, each taking 20 minutes.

2.7. Performance Evaluation

The evaluation of the system's performance was conducted based on two primary metrics: energy consumption and efficiency. Energy consumption (W) is the energy required to capture (i.e., separate and concentrate) one mole of CO_2, as calculated as follows:

$$W = \frac{\int_0^t UIdt}{\Delta n_{CO_2}} \quad (1)$$

where U (V) and I (A) are the cell potential and current, respectively, and Δn_{CO_2} (mol) is the number of moles of CO_2 desorbed during the experiment time of t. The current-time integral was calculated

using a built-in integral analysis by potentiostat software (Biologic; EC-Lab). Efficiency (η) indicated the percentage of theoretical CO_2 desorption that was achieved in the experiments:

$$\eta = \frac{\Delta n_{CO_2}}{\int_0^t Idt \times 2/F} \quad (2)$$

where F is the faraday constant (96,485 C/mol). The factor 2 in the denominator is used because, theoretically, two moles of protons are generated per mole of electron consumed, and each mole of proton can desorb one mole of CO_2 by shifting the bicarbonate equilibrium.

3. RESULTS AND DISCUSSION

3.1. Fundamental Electrochemical Analysis

This section presents detailed studies on the electrochemical fundamentals essential for the mechanisms and efficiencies of carbon capture through the proposed redox reactions. It covers thermodynamics, mass transfer, and kinetics of the system, with a thorough analysis of the operational conditions and optimizations required for enhanced electrochemical performance. This foundational understanding is critical for the bench-scale demonstration and the scalability of the technology.

3.1.1. Thermodynamic Analysis

To study the redox thermodynamic profile, CV experiments were performed separately for the vanadium and ferricyanide reactions. Figure 4A demonstrates the presence of multiple redox peaks for vanadium, suggesting the occurrence of different redox states of vanadium ions. Similar observations were reported in the VRFB literature [67–70]. To maximize the pH swing performance, it is essential to operate within a specific range of potential that includes only PCET reactions. Therefore, all of the observed peaks were labeled according to the literature [71], and suitable operational range of potential was decided to include only PCET reactions of vanadium. On the oxidation side (positive current), two peaks associated with the following reactions were observed:

$$VO^{2+} + H_2O \rightarrow VO_2^{+} + 2H^{+} + e^{-} \quad (3)$$

$$V^{3+} + H_2O \rightarrow VO^{2+} + 2H^{+} + e^{-} \quad (4)$$

Both reactions could be potentially desired as they are a PCET reaction, each producing two moles of H^+ per mole of electron transferred. This provides a higher pH swing capability compared to typical PCET reactions such as water splitting, which releases only one mole of H^+ per mole of electron [71]. Upon reduction (negative currents), VO_2^+, the product of reaction 3, was reversibly reduced back to VO^{2+}. In contrast, the reduction of VO^{2+}, the product of reaction 4, resulted in the formation of V^{3+}, which can be further reduced to V^{2+} via a non-PCET reaction, i.e., $V^{3+} + e \rightarrow V^{2+}$ (Figure 4A). Therefore, unlike reaction 3, which involves only reversible PCET reactions, the pathway of reaction 4 includes non-PCET reactions. Given this, the operating potential range was specifically set between 0.35 and 0.8 V (see Figure 4C) to prevent undesired reduction reactions involving V^{3+} and only include the reaction (3).

For the negolyte, CV measurements of ferrocyanide were conducted both with and without CO_2 purging (Figure 4B). The results indicate that the presence of CO_2-related species, such as carbonate and bicarbonate, does not affect the redox behavior of the $Fe(CN)_6^{3-}/Fe(CN)_6^{4-}$ pair (reaction 5):

$$Fe(CN)_6^{3-} + e^- \rightleftharpoons Fe(CN)_6^{4-} \qquad (5)$$

This is critical because any redox reactions involving CO_2 species could lead to parasitic reactions, thereby reducing the current efficiencies for carbon capture. Additionally, no other redox reactions, particularly PCET, were observed, ensuring that the protons transferred from the posolyte were exclusively utilized for CO_2 desorption.

The CV results from both the posolyte and negolyte solutions were combined to determine the minimum required Nernstian overpotential for the electrochemical system to function effectively (Figure 4C). Based on the CV results for vanadium (Figure 4A), a potential range of 0.35–0.8 V was selected to confine the vanadium speciation exclusively to VO^{2+}/VO_2^+ ions. The Nernstian overpotential was estimated to be 0.3 V.

3.1.2. Polarization Analysis

Following the CV analysis on the half-cell reactions separately, a series of CA experiments were conducted to study the current-potential profile of the system in a flow setup. These tests measured the response of the cell to different applied potentials, focusing on the anodic reaction of VO^{2+} oxidation and the cathodic reaction of $Fe(CN)_6^{3-}$ reduction. The resulting polarization curve is categorized into three primary regions in Figure 5A:

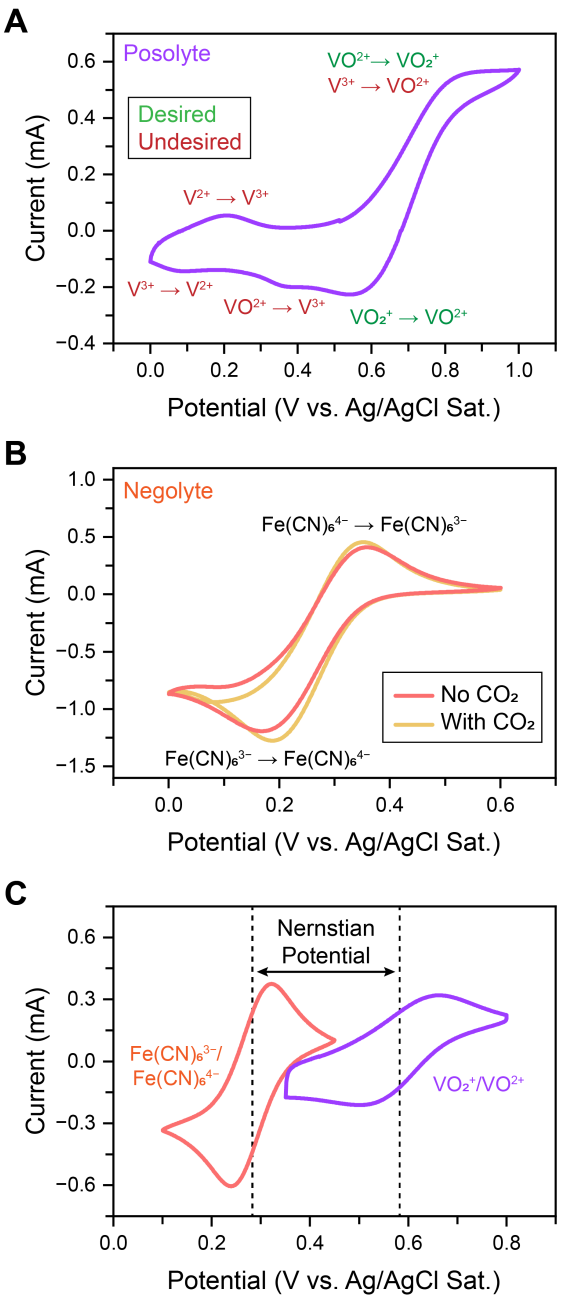

Figure 4. Cyclic voltammetry study of the posolyte and negolyte redox reactions (A) The Cyclic voltammetry (CV) profile of the posolyte redox reaction over a potential range of 0–1 V vs. Ag/AgCl Sat. reference electrode, where all peaks were identified and categorized as either desired or undesired. (B) The CV results of the negolyte redox reaction with and without CO_2 species, demonstrating that the presence of CO_2 does not affect the redox profile of the $Fe(CN)_6^{3-}/Fe(CN)_6^{4-}$ pair. (C) Combined CV profiles of the posolyte and negolyte, used to determine the Nernstian potential. The potential range for the posolyte redox (VO_2^+/VO^{2+}) was limited to include only the desired redox reactions.

(1) Activation Region: The increase in cell current corresponds with the cell potential from 0 to 0.5 V. This suggests that from the Nernstian potential, set at 0.3 V based on CV results, up to 0.5 V, the kinetics of the redox reactions determined the current levels. The relationship between current and potential in this range aligns with the Butler-Volmer equation [71,72], indicating a dependence on the activation energy required for the electrochemical reactions.

(2) Diffusion-Limited Region: Beyond the activation region, the current's response to increasing potential is at plateau, indicating that the rate of reaction is controlled by transport phenomena. This phase reflects a shift from reaction kinetics to mass transfer as the rate-limiting step.

(3) Ohmic Region: At higher potentials, specifically above 0.75 V, the current increases linearly with the cell potential, a characteristic of the ohmic region. This linear relationship is indicative of the electrolyte resistance becoming the main limiting factor to current flow.

To have an optimized potential for the CA tests in the desorption cycle, a cell potential of 0.5 V was selected. This potential is high enough to overcome the kinetic barriers and still avoid the unnecessary excess voltage due to diffusions, which results in higher energy consumption and potential degradation of the vanadium species.

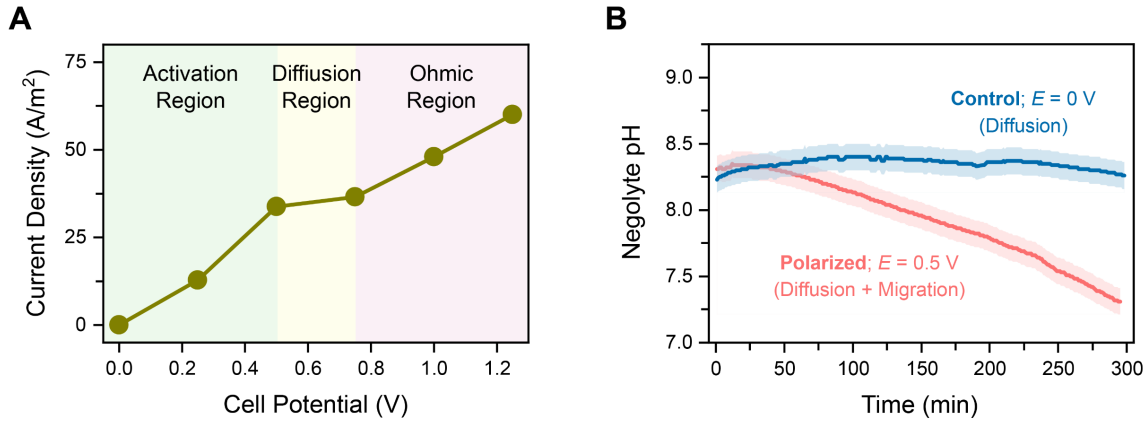

Figure 5. Polarization analysis and control experiment results. (A) A polarization profile was obtained by recording the stable current at various cell potentials during chronoamperometry (CA) experiments conducted at 0, 0.25, 0.5, 0.75, 1, 1.25, and 1.5 V. This analysis helped identify different overpotential regions, including activation, diffusion, and ohmic regions. (B) The impact of the applied potential (*E*) on proton transfer through the membrane was assessed by monitoring the negolyte pH. The polarized experiment at 0.5 V, which promotes mass transfer through both ion diffusion and migration, resulted in a significant pH change. In contrast, the control experiment at 0 V, reliant only on diffusion, showed no significant pH change. These results emphasize the minimal proton transfer due to diffusion alone and the crucial role of applied potential as the driving force for pH swing.

3.1.3. Mass Transfer Analysis

CA experiments were conducted by setting the applied potential at 0.5 V, as determined in the polarization experiment, to analyze the mass transfer phenomena within the cell. A parallel control experiment was performed without any applied potential, during which the pH and DIC content of the negolyte were monitored. The CA results reveal the combined impacts of proton ion migration and diffusion, whereas the control experiment elucidates the contribution of diffusion alone to the overall mass transfer.

The results indicate that the negolyte pH decreased during the CA experiment, while no significant pH change was observed in the controlled experiment without an applied potential (Figure 5B). This clearly demonstrates that the migration contribution induced by the applied potential is the primary driving force for proton transfer and the resultant pH swing. Despite the pH gradient across the membrane, the contribution of spontaneous proton ion diffusion was found to be negligible (according to the controlled experiment), ensuring minimal unwanted self-discharge of the electrochemical cell. Furthermore, sampling and titration showed no DIC removal in the control experiment.

To further study the transport phenomena by migration and its relation to the solution chemistry, several desorption experiments were carried out with varying concentrations of K_2SO_4 as the background electrolyte, while keeping the $K_3Fe(CN)_6$, $VOSO_4$, and the initial CO_2 loading constant. The addition of background electrolyte with non-redox active ions enhanced the overall conductivity of the solution. This led to a reduction in ohmic resistance (R_{ohmic}; combination of solution and membrane resistances), resulting in higher current densities (Figure 6A). This observation aligns with the transport principles outlined in the Nernst-Planck equation, which describes ion movement in response to concentration gradients and electric fields. Increasing the background electrolyte concentration beyond 0.3 M did not further increase the current density, as the favorable effects of adding a background electrolyte to reduce the ohmic resistance were likely offset by an increase in reaction resistance. Similar results were observed in the literature, concluding that increasing the background electrolyte concentration beyond a certain threshold can result in interference of the non-redox ions with the redox reactions on the electrode, thereby increasing the reaction resistance [73].

Furthermore, the increase in the concentration of the background electrolyte resulted in a decrease in CO_2 desorption efficiency, as shown in Figure 6B. This inverse relationship suggests that while higher background ion concentrations improve conductivity and current flow, they also hinder the system's primary objective—efficient CO_2 desorption. This is due to the competition between protons and K^+ ions over migration through the PEM. Proton transfer is crucial for increasing the efficiency of CO_2 desorption by reducing the pH of the negolyte. However, the larger concentration of K^+ ions provide a competing mechanism that can reduce the system's desorption capabilities. Therefore, there is a key balance between enhancing the current by increasing the concentration of background electrolyte and maintaining a high CO_2 desorption efficiency.

Both the current density and desorption efficiency directly influence the CO_2 desorption flow rate. The average flow rate of desorbed CO_2 initially increased with the addition of background electrolyte but then declined at concentrations exceeding 0.1 M (Figure 6B). This result indicates that initially, the favorable impact of increasing electrolyte concentration on current density enhances the desorption flow rate; however, beyond 0.1 M, this benefit is mainly offset by the decreased desorption efficiency. Therefore, the background concentration of 0.1 M was found to be the optimal point for maximizing the system’s performance. This concentration was used for the subsequent experiments, reflecting the optimal initial concentration ratio of 1:1 for the redox active species and background electrolyte.

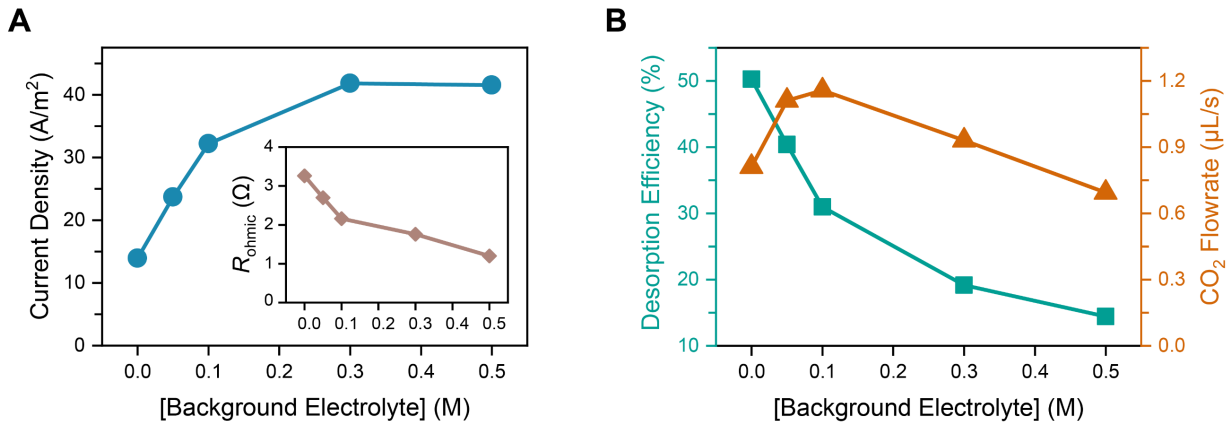

Figure 6. The impact of the background electrolyte concentration on the desorption performance. The impacts of the background electrolyte on (A) current density and ohmic resistance (R_{ohmic}; inset), and (B) desorption efficiency and CO_2 desorption flowrate.

3.1.4. Electrode Kinetics Improvement

The kinetics of the redox reaction is a critical factor that directly influences the energetics of carbon capture. To enhance these kinetics, we implemented an electrode treatment process. Previous studies have investigated thermal, chemical, and plasma modifications to improve the kinetic performance of electrodes in VRFBs [61,74]. Among these, plasma treatment has shown promise in enhancing electrode performance [60]. This improvement is attributed to an increase in the electrode's active surface area and the introduction of surface oxygen [68] and nitrogen [75] functional groups, which enhance the hydrophilicity of carbon electrodes [60]. Building on this foundation, we also adopted a plasma-based method to treat the graphite electrodes, aiming to enhance their kinetic performance.

CA was conducted to evaluate the impact of plasma treatment on the electrodes. The results demonstrated a 33% increase in current density and a 19% improvement in desorption efficiency (Figure 6A). The enhanced current achieved by the treated electrode is explained by EIS results. The ohmic resistances (R_{ohmic}), including solution and membrane resistances, remained unchanged, as the treatment process does not affect the mass transfer characteristics of the system. However, the charge transfer resistance (R_{ct}), which reflects electrode kinetics, was significantly reduced for the treated electrode (0.04 Ω) compared to the untreated electrode (0.07 Ω) (Figure 6B). Thus, the lower overall resistance of the treated sample, stemming from reduced charge transfer resistance, contributed to the observed higher current density relative to the untreated sample.

The reduced charge transfer resistance observed in the treated sample can be attributed to the enhanced hydrophilicity of the electrode surface. This improvement was confirmed by contact angle measurements. For the untreated sample, the contact angle between the graphite electrode and an aqueous solution was approximately 90 degrees (Figure 6C), indicating low hydrophilicity. After plasma treatment, a significant increase in hydrophilicity was evident, with the contact angle reducing to below 10 degrees (Figure 6D). Overall, the treated electrode exhibited improved

hydrophilicity, which led to a reduction in charge transfer resistance (kinetics) and ultimately enhanced the current density.

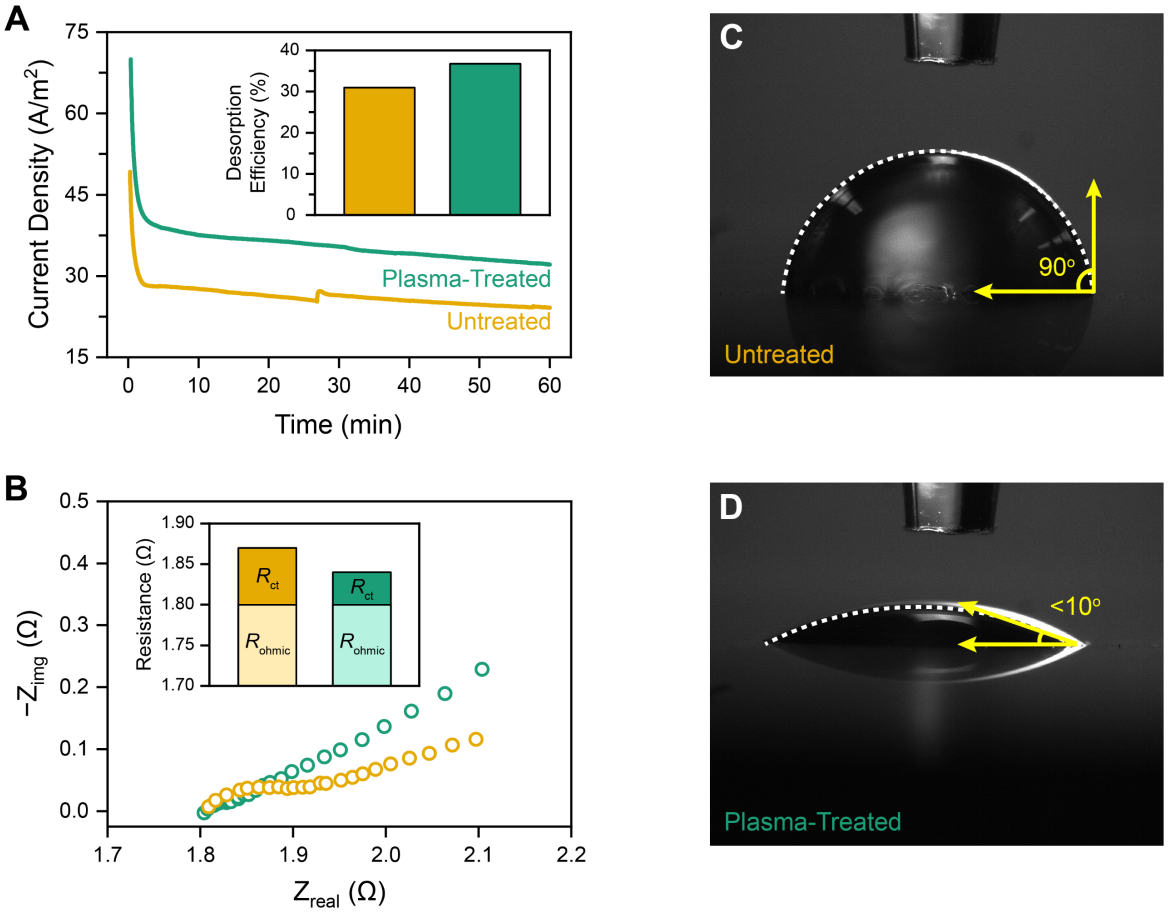

Figure 7. Impact of plasma treatment on electrode kinetics. (A) Comparison of current density and desorption efficiency (inset) between plasma-treated and untreated samples. (B) Nyquist plots from the electrochemical impedance spectroscopy (EIS) measurements comparing treated versus untreated samples. The resistance components, including ohmic resistance (R_{ohmic}) and charge transfer resistance (R_{ct}), were calculated using a Randles equivalent circuit (inset). (C-D) Hydrophilicity assessments of electrode surfaces using high-resolution contact angle measurements for (C) untreated and (D) plasma-treated samples.

3.2. Bench-scale Demonstration and Performance Evaluation

The results from the fundamental electrochemical analysis detailed in the previous section informed the bench-scale demonstration of the integrated carbon capture process. In this context, the system's efficacy in CO_2 desorption and absorbent regeneration was evaluated during simulated day and night cycles. Additionally, the reversibility of the system across multiple cycles was analyzed to evaluate long-term stability. Finally, the energetics of the process were estimated and compared with those of other proposed technologies.

3.2.1. Bench Scale Operation

The bench-scale operation of the system is comprised of two sequential stages: (1) CO_2 desorption, achieved by increasing the SOC, and (2) absorbent regeneration, accomplished by decreasing the SOC (Figure 8). During the desorption cycle, which is proposed for daytime operation, a constant potential of 0.5 V was applied to the cell. This potential, determined from the polarization analysis, facilitated the consumption of VO^{2+} in the posolyte and consequently increased the SOC (Figure 8A). In the negolyte, $Fe(CN)_6^{3-}$ was reduced to $Fe(CN)_6^{4-}$. The generated current density in this cycle averaged 60 A/m^2. As the cycle progressed, the current density decreased to approximately 20 A/m^2, at which point the desorption cycle was terminated (Figure 8B). The observed drop in current can be attributed to the decreasing concentration of VO^{2+} and the increasing concentrations of VO_2^+ and protons, which collectively elevate the Nernstian overpotential. This current represented the optimal SOC of 70%. Attempts to push the process to higher SOCs were also pursued (results not shown here), which proved to be less efficient. As evident from Figure 8A, the SOC profile is expected to reach a plateau, indicating a less efficient process with increased energy requirements beyond an SOC of 70%. During this cycle, OCP increased from 0 to 0.5 V, similar to the battery charge cycle, indicating an energy storage potential application of the system.

Throughout the desorption cycle, the pH of the posolyte decreased from 2.7 to 1.51 due to proton generation in the PCET reaction of VO^{2+} oxidation to VO_2^+. Conversely, the pH of the negolyte, which serves as the proton receiver, dropped from 8.6 to 7.6, as illustrated in Figure 8C. The negolyte pH was influenced by two factors: (1) the proton receiving rate from the posolyte, which decreases the negolyte pH, and (2) CO_2 desorption, which tends to increase the solution pH. At the beginning of the cycle, the effects of CO_2 outgassing and proton reception offset each other due to the absence of significant proton accumulation, resulting in a relatively stable pH. However, as the cycle progresses beyond a SOC of 30%, proton accumulation becomes predominant, leading to a decrease in the solution pH. The decreased pH of the negolyte obtained during daytime operation facilitated CO_2 desorption, with an average desorption efficiency of 50%, consistent with the value observed in the fundamental analysis. The source of inefficiency is likely related to the transfer of competing cations through the membrane, rather than protons. Future investigations will focus on enhancing membrane selectivity and adjusting operational parameters to improve the proton transfer rate and, consequently, the CO_2 desorption efficiency.

To regenerate the VO^{2+} and $Fe(CN)_6^{3-}$ species (absorbent regeneration step), a reverse polarization of −0.5 V was applied to the cell during the proposed night-time cycle. This process continued until the SOC reached 20%, at which point the current density dropped to approximately −20 A/m^2. The average current density obtained in this stage (~30 A/m^2) was lower than that observed in the desorption cycle. This difference can be attributed to the slower kinetics of the regeneration stage compared to the desorption cycle. Despite the lower current density, an effective increase in the negolyte pH level was obtained, regenerating the absorbent solution. The negolyte pH increased from 7.6 to 8.6, which was the initial value at the beginning of the desorption experiment (Figure 8C). Therefore, the developed bench-scale process successfully achieved the required pH swing for CO_2 desorption and absorbent regeneration.

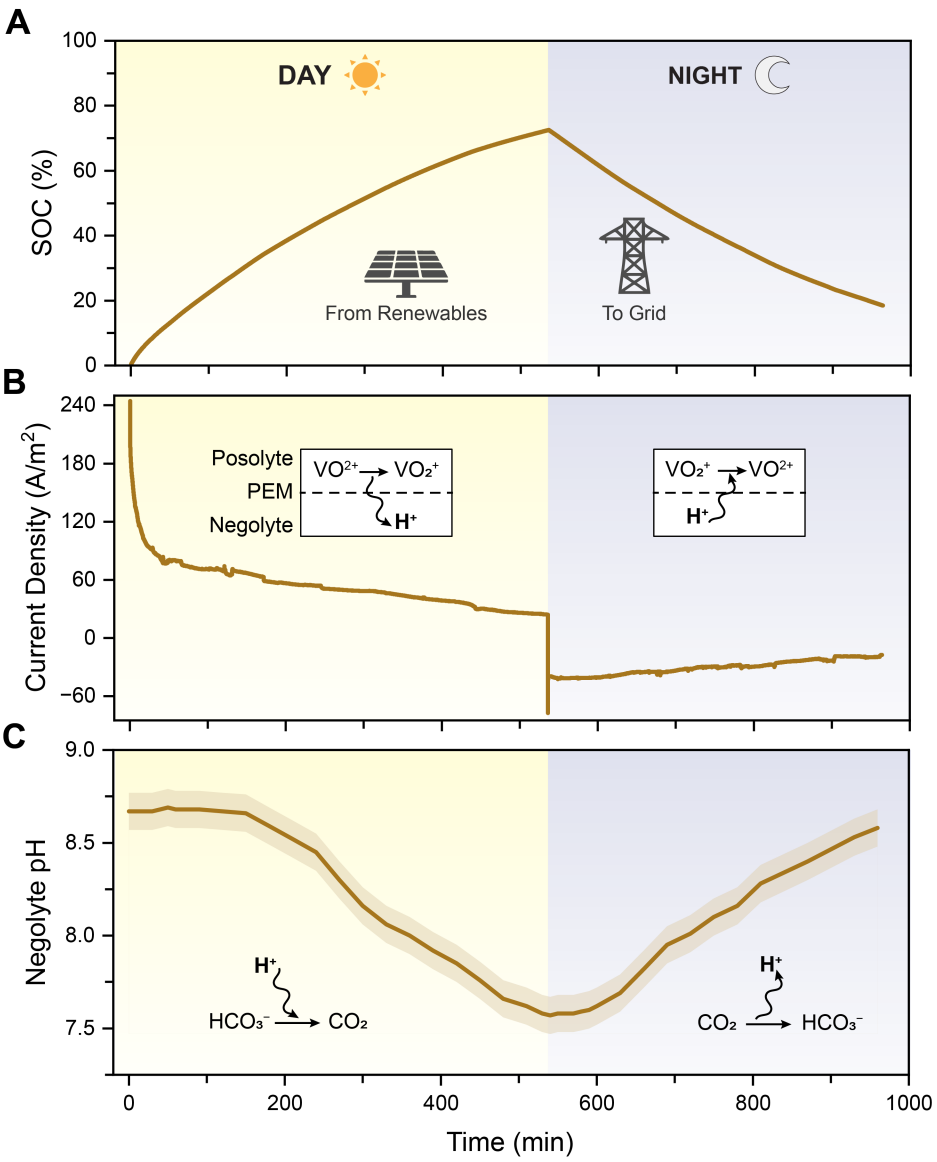

Figure 8. Bench-scale operation of the cell in Day-Night mode. (A) Chronoamperometry (CA) was conducted at a cell potential of 0.5 V during daytime operation to increase the state of charge (SOC) to 70%, followed by a decrease in SOC during nighttime operation. (B-C) Monitoring of (B) current and (C) negolyte pH, which reflects the proton transfer to the negolyte for CO_2 desorption during the daytime, and the withdrawal of protons from the negolyte compartment for absorbent regeneration during the nighttime.

3.2.2. Reversibility in Cycles

Reversibility, a critical parameter for the stability and durability of electrochemical flow systems, was evaluated through cyclic operation of the redox reactions in the proposed process. The applied cell potential was changed from 0.5 V to −0.5 V repeatedly to assess the reversibility of the anodic and cathodic reactions. The observations over 20 half-cycles, equivalent to 10 complete day-night cycles, revealed a consistent current profile, suggesting minimal degradation

or alteration in the reaction efficiency (Figure 9). The redox pairings of both VO_2^+/VO^{2+} and $Fe(CN)_6^{3-}/Fe(CN)_6^{4-}$ exhibited reversibility, indicating that the system has the potential for stable operation over multiple cycles with future investigations.

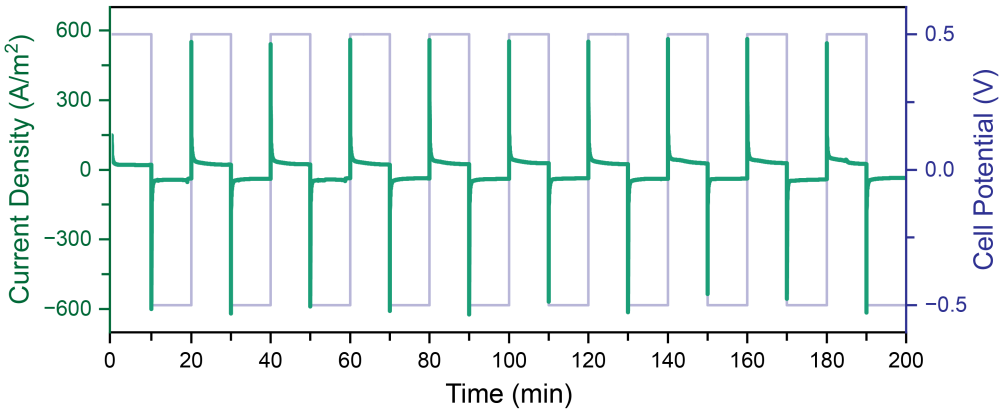

Figure 9. Reversibility of the redox reaction over multiple cycles. Chronoamperometry (CA) was conducted to evaluate the reversibility of the day-night cycles. The cell potential was alternated between 0.5 V for the proposed daytime and −0.5 V for the proposed nighttime operations. This reversibility test was carried out over 20 day-night cycles.

3.2.3. Energetics Analysis

Energetics is identified as one of the primary performance metrics for any technology developed for carbon capture applications. The developed system can store energy during daytime CO_2 desorption operations and releasing it during nighttime absorbent regeneration. To calculate the net energy consumption of the developed process, the energy harvested at night was subtracted from the energy consumed during the day. Specifically, 98 kJ/mol CO_2 was consumed during desorption, with 44 kJ subsequently stored and harvested during the regeneration stage. Thus, the net energy consumption of the process was calculated as 54 kJ/mol CO_2 (Figure 10A). The minimum required energy was calculated at 24 kJ/mol CO_2 for a faradic efficiency of 100%, assuming all the generated protons from the PCET reaction will migrate to negolyte to drive CO_2 desorption. The disparity between the experimental energy consumption and the minimum thermodynamic energy consumption can be attributed to the desorption efficiency of the process, which averaged 50%. This indicates that only half of the protons generated by the PCET reaction are transferred to the negolyte (desorption chamber), hence only half of the energy consumption effectively contributes to CO_2 desorption. This explains why experimental energetics is twice as high as the minimum thermodynamic energetics. An important area for future research would be enhancing desorption efficiency through the development of membranes with improved selectivity that offer higher proton transfer rates and fine-tuning operational parameters.

The energetics of the developed system were compared with other ECC technologies, particularly those utilizing the pH swing mechanism. As previously discussed, three types of electrochemical pH swing processes have been developed: redox-mediated, membrane electrodialysis (MED), and proton concentration process (PCP). The energetics of the developed process proved very competitive with those of the redox-mediated pH swing processes. By aggregating the results

from several redox-mediated processes developed in recent years, an average energy consumption of 55 kJ/mol CO_2 was observed (Figure 10B). Various PCET redox-active compounds have been explored, with notable recent examples including 3,3′-(phenazine-2,3-diylbis(oxy))bis(propane-1-sulfonate) (DSPZ) [51], 7,8-dihydroxyphenazine-2-sulfonic acid (DHPS) [50], riboflavin derivatives [76], and phenazine derivatives [53]. The net energy consumption of the developed process was also competitive with those of the MED and PCP systems, which averaged 72 kJ/mol CO_2 and 54 kJ/mol CO_2, respectively (Figure 10B). This comparison is based on aggregating results from various configurations of these systems.

The energetics of the developed process were further compared to other ECC approaches, namely EMAR and EGN. The EMAR technology, employing various configurations of metal and amine absorbents, achieved an average energy consumption of 60 kJ/mol CO_2 [33,36,77]. EGN systems, which utilize redox molecules like quinones that form CO_2 adducts upon reduction, exhibited an average energy consumption of 71 kJ/mol CO_2 (Figure 10B) [19,20,78,79]. Therefore, the developed system demonstrates competitive energetics when compared to both EMAR and EGN technologies.

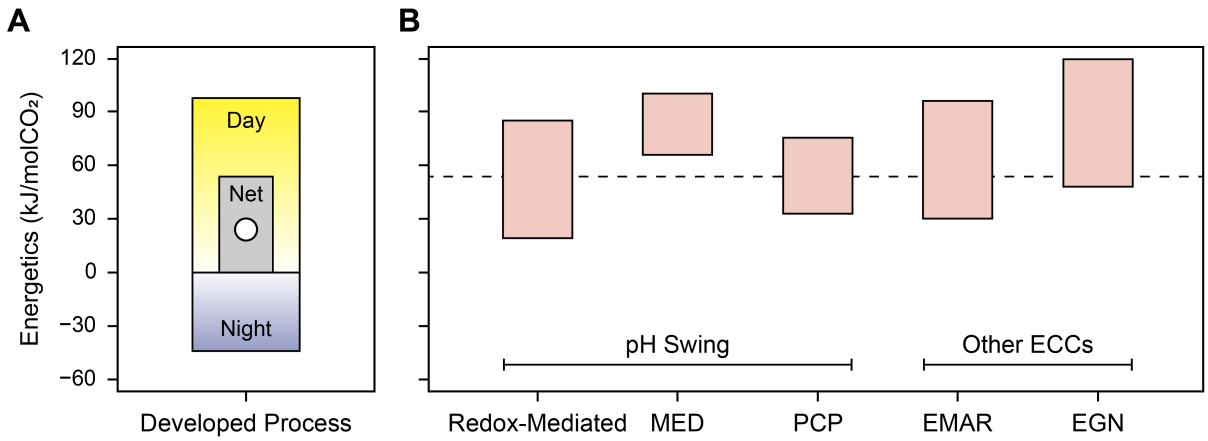

Figure 10. Energetics Analysis of the system. (A) Energy consumption of the cell during desorption (day) cycle was calculated at 98 kJ/mol CO_2 from the current-time integration. The harvested energy during absorbent regeneration (night) cycle was calculated at 44 kJ/mol CO_2 from current-time integration. Net energy consumption of the cell was calculated at 54 kJ/mol CO_2 by subtracting the harvested energy from the consumed energy. The minimum required energy was calculated at 24 kJ/mol CO_2 (circle symbol) for a faradic efficiency of 100%, assuming all the generated protons from the PCET reaction will migrate to negolyte to drive CO_2 desorption. (B) Comparison of the net energy requirement of the proposed process (dashed line) with other electrochemical carbon capture technologies. The energy consumption of the developed system is compared to other electrochemical processes, including pH swing systems (redox-mediated, membrane electrodialysis (MED), and proton concentration process (PCP)), electrochemically mediated amine regeneration (EMAR), and quinone-based electrochemical generation of nucleophiles (EGN). For each process, the graph was constructed based on the range of experimental energy values reported in the literature to separate CO_2 from simulated industrial flue gas streams.

Besides competitive energetics, the developed process offers several other advantages. Firstly, it does not require electrode materials based on precious metals, which are commonly used in other pH swing processes such as redox-mediated and MED systems [4,43,48]. Secondly, the

system is fully insensitive to the presence of oxygen in the flue gas, a significant issue reported in both redox-mediated pH swing and EGN systems [51,57,4,56]. Thirdly, the process is inspired by VRFBs, which is advantageous for process scale-up [61,67,69,70]. Expertise in scaling up VRFBs can be effectively applied to scaling and implementing this developed carbon capture system. Additionally, the solubilities of the redox-active compounds used (vanadium salts) are significantly higher than those used in other redox-mediated pH swing processes (e.g. quinones), which enhances the CO_2 cyclic capture capacity. Lastly, and perhaps most significantly, the developed system has the capability to store energy and function as a battery during the absorbent regeneration process, allowing for operation in a day-night mode. These advantages collectively highlight the substantial potential of the developed process.

4. CONCLUSIONS

This study introduced a novel method for electrochemical carbon capture through pH swing, using the widely recognized vanadium and ferricyanide redox reactions and potassium carbonate absorbent. The developed system enables controlled cycles of CO_2 desorption and absorbent regeneration. During daytime, when solar electricity is available, the system desorbs CO_2 and stores electrical energy, while during nighttime, when solar energy is not available, the system discharges electricity while regenerating the absorbent.

A comprehensive investigation including the analysis of redox thermodynamics, kinetics, and transport phenomena was conducted, and a bench-scale operation of the system along with reversibility over multiple cycles was demonstrated. Through fundamental thermodynamic analysis, the Nernstian potential was identified as 0.3 V. Further polarization tests indicated that the practical operational potential needs to be at least 0.5 V to overcome the activation barrier. Examining the fundamentals of mass transfer and solution chemistry, a detailed relationship between conductivity enhancement and desorption efficiency was revealed. While higher electrolyte concentrations facilitated improved conductivity, they also introduced competing ion migration dynamics that could hinder CO_2 desorption. Therefore, a concentration ratio of 1:1 between the redox active species and background electrolyte was selected for the system operation. Plasma treatment was used to improve electrode kinetics. The results indicated an increase in electrode hydrophilicity, leading to a 43% reduction in charge transfer resistance.

The bench-scale demonstration confirmed the system's capability of carrying out CO_2 desorption and absorbent regeneration cycles, as well as confirming its reversibility over several cycles. The energetics' study indicated that the developed technology is competitive compared to the other ECC technologies, with a net energy consumption of 54 kJ/mol CO_2. The proposed system offers several advantages in addition to competitive energetics. Firstly, it features a decoupling of the PCET reaction compartment from the chamber exposed to flue gas, which mitigates the negative impact of gas phase impurities, particularly O_2, unlike existing redox-mediated pH-swing systems. Secondly, the proton pump interface effectively addresses potential issues related to Nernstian overpotentials caused by proton accumulation, as it actively transfers the generated ions. Thirdly, the solubility of the redox-active species in our system does not pose a limitation as it might with

quinones. Lastly, the process inherits the established VRFBs' capability to store and harvest energy.

While the results of this study are promising, further research is necessary to optimize the performance of the system and overcome existing challenges. Future efforts should focus on enhancing membrane selectivity, mitigating losses at interfaces, and investigating the effects of higher electrolyte concentrations to improve the energetics. Additionally, detailed battery characterizations and assessments of scaling potential are critical to determine the feasibility of industrial-scale deployment.

AKNOWLEDGMENTS

The authors acknowledge the University of Houston's Division of Research (UH DOR) for the new faculty startup package granted to Dr. Rahimi. We also express our gratitude for the support received from the High Priority Area Research Seed Grant provided by the UH DOR (Award Number: I0511686). Additionally, we acknowledge the support from the Department of Energy (DOE; Award Number: DE-FE-0032408). We are also grateful to Dr. Pooria Tajalli and Dr. T. Randall Lee from the Department of Chemistry at UH for their assistance with the electrode plasma treatment and contact angle measurements.

REFERENCES

1. Assessing the Global Climate in 2023 [Internet]. National Centers for Environmental Information (NCEI)2024 [cited 2024 May 2];Available from: https://www.ncei.noaa.gov/news/global-climate-202312

2. Masson-Delmotte V, Zhai P, Pirani A, Connors SL, Péan C, Berger S, et al., editors. Climate Change 2021: The Physical Science Basis. Contribution of Working Group I to the Sixth Assessment Report of the Intergovernmental Panel on Climate Change. Cambridge, United Kingdom and New York, NY, USA: Cambridge University Press; 2021.

3. Rogelj J, den Elzen M, Höhne N, Fransen T, Fekete H, Winkler H, et al. Paris Agreement climate proposals need a boost to keep warming well below 2 °C. Nature 2016;534:631–9.

4. Rahimi M, Khurram A, Hatton TA, Gallant B. Electrochemical carbon capture processes for mitigation of CO2 emissions. Chem. Soc. Rev. 2022;51:8676–95.

5. Aleta P, Refaie A, Afshari M, Hassan A, Rahimi M. Direct ocean capture: the emergence of electrochemical processes for oceanic carbon removal. Energy Environ. Sci. 2023;16:4944–67.

6. Rahimi M. Public Awareness: What Climate Change Scientists Should Consider. Sustainability 2020;12:8369.

7. Bui M, Adjiman CS, Bardow A, Anthony EJ, Boston A, Brown S, et al. Carbon capture and storage (CCS): the way forward. Energy Environ. Sci. 2018;11:1062–176.

8. Martin-Roberts E, Scott V, Flude S, Johnson G, Haszeldine RS, Gilfillan S. Carbon capture and storage at the end of a lost decade. One Earth 2021;4:1569–84.

9. Rochelle GT. Amine Scrubbing for CO2 Capture. Science 2009;325:1652–4.

10. Liang Z (Henry), Rongwong W, Liu H, Fu K, Gao H, Cao F, et al. Recent progress and new developments in post-combustion carbon-capture technology with amine based solvents. International Journal of Greenhouse Gas Control 2015;40:26–54.

11. Rahimi M, Moosavi SM, Smit B, Hatton TA. Toward smart carbon capture with machine learning. Cell Reports Physical Science 2021;2:100396.

12. Haszeldine RS. Carbon Capture and Storage: How Green Can Black Be? Science 2009;325:1647–52.

13. Dutcher B, Fan M, Russell AG. Amine-Based CO2 Capture Technology Development from the Beginning of 2013—A Review. ACS Appl. Mater. Interfaces 2015;7:2137–48.

14. Porter RTJ, Fairweather M, Kolster C, Mac Dowell N, Shah N, Woolley RM. Cost and performance of some carbon capture technology options for producing different quality CO2 product streams. International Journal of Greenhouse Gas Control 2017;57:185–95.

15. Sharifian R, Wagterveld RM, Digdaya IA, Xiang C, Vermaas DA. Electrochemical carbon dioxide capture to close the carbon cycle. Energy Environ. Sci. 2021;14:781–814.

16. Renfrew SE, Starr DE, Strasser P. Electrochemical Approaches toward CO2 Capture and Concentration. ACS Catal. 2020;10:13058–74.

17. Zito AM, Clarke LE, Barlow JM, Bím D, Zhang Z, Ripley KM, et al. Electrochemical Carbon Dioxide Capture and Concentration. Chem. Rev. 2023;123:8069–98.

18. Shaw RA, Hatton TA. Electrochemical CO2 capture thermodynamics. International Journal of Greenhouse Gas Control 2020;95:102878.

19. Rheinhardt JH, Singh P, Tarakeshwar P, Buttry DA. Electrochemical Capture and Release of Carbon Dioxide. ACS Energy Lett. 2017;2:454–61.

20. Apaydin DH, Głowacki ED, Portenkirchner E, Sariciftci NS. Direct Electrochemical Capture and Release of Carbon Dioxide Using an Industrial Organic Pigment: Quinacridone. Angewandte Chemie International Edition 2014;53:6819–22.

21. Mizen MB, Wrighton MS. Reductive Addition of CO 2 to 9,10-Phenanthrenequinone. J. Electrochem. Soc. 1989;136:941.

22. Kang JS, Kim S, Hatton TA. Redox-responsive sorbents and mediators for electrochemically based CO2 capture. Current Opinion in Green and Sustainable Chemistry 2021;31:100504.

23. Schimanofsky C, Wielend D, Kröll S, Lerch S, Werner D, Gallmetzer JM, et al. Direct Electrochemical CO2 Capture Using Substituted Anthraquinones in Homogeneous Solutions: A Joint Experimental and Theoretical Study. J. Phys. Chem. C 2022;126:14138–54.

24. Bui AT, Hartley NA, Thom AJW, Forse AC. Trade-Off between Redox Potential and the Strength of Electrochemical CO2 Capture in Quinones. J. Phys. Chem. C 2022;126:14163–72.

25. Legrand L, Schaetzle O, de Kler RCF, Hamelers HVM. Solvent-Free CO2 Capture Using Membrane Capacitive Deionization. Environ. Sci. Technol. 2018;52:9478–85.

26. Kokoszka B, Jarrah NK, Liu C, Moore DT, Landskron K. Supercapacitive Swing Adsorption of Carbon Dioxide. Angewandte Chemie International Edition 2014;53:3698–701.

27. Liu C, Landskron K. Design, construction, and testing of a supercapacitive swing adsorption module for CO2 separation. Chem. Commun. 2017;53:3661–4.

28. Binford TB, Mapstone G, Temprano I, Forse AC. Enhancing the capacity of supercapacitive swing adsorption CO2 capture by tuning charging protocols. Nanoscale 2022;14:7980–4.

29. Lamb KJ, Dowsett MR, Chatzipanagis K, Scullion ZW, Kröger R, Lee JD, et al. Capacitance-Assisted Sustainable Electrochemical Carbon Dioxide Mineralisation. ChemSusChem 2018;11:137–48.

30. Dowsett MR, Lewis CM, North M, Parkin A. Exploring the scope of capacitance-assisted electrochemical carbon dioxide capture. Dalton Trans. 2018;47:10447–52.

31. C. Stern M, Simeon F, Herzog H, Alan Hatton T. Post- combustion carbon dioxide capture using electrochemically mediated amine regeneration. Energy & Environmental Science 2013;6:2505–17.

32. Stern MC, Hatton TA. Bench-scale demonstration of CO2 capture with electrochemically-mediated amine regeneration. RSC Adv. 2014;4:5906–14.

33. Wang M, Rahimi M, Kumar A, Hariharan S, Choi W, Hatton TA. Flue gas CO2 capture via electrochemically mediated amine regeneration: System design and performance. Applied energy 2019;255:113879.

34. Rahimi M, Diederichsen KM, Ozbek N, Wang M, Choi W, Hatton TA. An Electrochemically Mediated Amine Regeneration Process with a Mixed Absorbent for Postcombustion CO2 Capture. Environ. Sci. Technol. 2020;54:8999–9007.

35. Rahimi M, Zucchelli F, Puccini M, Alan Hatton T. Improved CO2 Capture Performance of Electrochemically Mediated Amine Regeneration Processes with Ionic Surfactant Additives. ACS Appl. Energy Mater. 2020;3:10823–30.

36. Hassan A, Refaie A, Aleta P, Afshari M, Kalantari E, Fang Y, et al. Reviving the absorbent chemistry of electrochemically mediated amine regeneration for improved point source carbon capture. Chemical Engineering Journal 2024;484:149566.

37. Jin S, Wu M, Jing Y, Gordon RG, Aziz MJ. Low energy carbon capture via electrochemically induced pH swing with electrochemical rebalancing. Nat Commun 2022;13:2140.

38. Zhou C, Ni J, Chen H, Guan X. Harnessing electrochemical pH gradient for direct air capture with hydrogen and oxygen by-products in a calcium-based loop. Sustainable Energy Fuels 2021;5:4355–67.

39. Datta S, Henry MP, Lin YuPoJ, Fracaro AT, Millard CS, Snyder SW, et al. Electrochemical CO2 Capture Using Resin-Wafer Electrodeionization. Ind. Eng. Chem. Res. 2013;52:15177–86.

40. Eisaman MD, Alvarado L, Larner D, Wang P, Garg B, Littau KA. CO2 separation using bipolar membrane electrodialysis. Energy Environ. Sci. 2011;4:1319–28.

41. Oloye O, O'Mullane AP. Electrochemical Capture and Storage of CO2 as Calcium Carbonate. ChemSusChem 2021;14:1767–75.

42. Eisaman MD, Alvarado L, Larner D, Wang P, Littau KA. CO2 desorption using high-pressure bipolar membrane electrodialysis. Energy Environ. Sci. 2011;4:4031–7.

43. Watkins JD, Siefert NS, Zhou X, Myers CR, Kitchin JR, Hopkinson DP, et al. Redox-Mediated Separation of Carbon Dioxide from Flue Gas. Energy Fuels 2015;29:7508–15.

44. Straatman PJT, van Sark WGJHM. Indirect air CO2 capture and refinement based on OTEC seawater outgassing. iScience 2021;24:102754.

45. Gilliam RJ, Boggs BK, Decker V, Kostowskyj MA, Gorer S, Albrecht TA, et al. Low Voltage Electrochemical Process for Direct Carbon Dioxide Sequestration. J. Electrochem. Soc. 2012;159:B627.

46. Mehmood A, Iqbal MI, Lee JY, Hwang J, Jung KD, Ha HY. A novel high performance configuration of electrochemical cell to produce alkali for sequestration of carbon dioxide. Electrochimica Acta 2016;219:655–63.

47. Littau K, Torres FE. System and method for recovery of CO2 by aqueous carbonate flue gas capture and high efficiency bipolar membrane electrodialysis. US Patent Pending [Internet] 2013 [cited 2024 May 5];Available from: https://www.freepatentsonline.com/8535502.html

48. Eisaman M, Schwartz D, Amic S, Larner D, Zesch J, Torres F, et al. Energy-efficient electrochemical CO 2 capture from the atmosphere. Technical Proceedings of the 2009 NSTI Nanotechnology Conference and Expo, NSTI-Nanotech 2009 2009;3.

49. Huang C, Liu C, Wu K, Yue H, Tang S, Lu H, et al. CO2 Capture from Flue Gas Using an Electrochemically Reversible Hydroquinone/Quinone Solution. Energy Fuels 2019;33:3380–9.

50. Xie H, Wu Y, Liu T, Wang F, Chen B, Liang B. Low-energy-consumption electrochemical CO2 capture driven by biomimetic phenazine derivatives redox medium. Applied Energy 2020;259:114119.

51. Jin S, Wu M, Gordon RG, Aziz MJ, Kwabi DG. pH swing cycle for CO2 capture electrochemically driven through proton-coupled electron transfer. Energy Environ. Sci. 2020;13:3706–22.

52. Seo H, Rahimi M, Hatton TA. Electrochemical Carbon Dioxide Capture and Release with a Redox-Active Amine. J. Am. Chem. Soc. 2022;144:2164–70.

53. Pang S, Jin S, Yang F, Alberts M, Li L, Xi D, et al. A phenazine-based high-capacity and high-stability electrochemical CO2 capture cell with coupled electricity storage. Nat Energy 2023;8:1126–36.

54. Rahimi M, Catalini G, Hariharan S, Wang M, Puccini M, Hatton TA. Carbon Dioxide Capture Using an Electrochemically Driven Proton Concentration Process. Cell Reports Physical Science 2020;1:100033.

55. Rahimi M, Catalini G, Puccini M, Alan Hatton T. Bench-scale demonstration of CO 2 capture with an electrochemically driven proton concentration process. RSC Advances 2020;10:16832–43.

56. Li X, Mathur A, Liu A, Liu Y. Electrifying Carbon Capture by Developing Nanomaterials at the Interface of Molecular and Process Engineering. Acc. Chem. Res. 2023;56:2763–75.

57. Barlow JM, Clarke LE, Zhang Z, Bím D, Ripley KM, Zito A, et al. Molecular design of redox carriers for electrochemical CO2 capture and concentration. Chem. Soc. Rev. 2022;51:8415–33.

58. Barlow JM, Yang JY. Oxygen-Stable Electrochemical CO2 Capture and Concentration with Quinones Using Alcohol Additives. J. Am. Chem. Soc. 2022;144:14161–9.

59. Fell EM, Porcellinis DD, Jing Y, Gutierrez-Venegas V, George TY, Gordon RG, et al. Long-Term Stability of Ferri-/Ferrocyanide as an Electroactive Component for Redox Flow Battery Applications: On the Origin of Apparent Capacity Fade. J. Electrochem. Soc. 2023;170:070525.

60. Hammer EM, Berger B, Komsiyska L. Improvement of the Performance of Graphite Felt Electrodes for Vanadium-Redox-Flow-Batteries by Plasma Treatment. International Journal of Renewable Energy Development 2014;3:7–12.

61. Kim KJ, Park MS, Kim YJ, Kim JH, Dou SX, Skyllas-Kazacos M. A technology review of electrodes and reaction mechanisms in vanadium redox flow batteries. J. Mater. Chem. A 2015;3:16913–33.

62. Tajalli P, Hernandez Rivera JM, Omidiyan M, Tran HV, Lee TR. Carbonate-Terminated Self-Assembled Monolayers for Mimicking Nanoscale Polycarbonate Surfaces. ACS Appl. Nano Mater. 2023;6:2472–7.

63. Tajalli P, Omidiyan M, Rahimi MM, Lee TR. Exploring the potential of transition-metal-based hollow micro- and nanoparticles in supercapacitor electrodes. Materials Today Sustainability 2024;26:100733.

64. Rahimi M, Zhu L, Kowalski KL, Zhu X, Gorski CA, Hickner MA, et al. Improved electrical power production of thermally regenerative batteries using a poly(phenylene oxide) based anion exchange membrane. Journal of Power Sources 2017;342:956–63.

65. Rahimi M, D'Angelo A, Gorski CA, Scialdone O, Logan BE. Electrical power production from low-grade waste heat using a thermally regenerative ethylenediamine battery. Journal of Power Sources 2017;351:45–50.

66. Rahimi M, Kim T, Gorski CA, Logan BE. A thermally regenerative ammonia battery with carbon-silver electrodes for converting low-grade waste heat to electricity. Journal of Power Sources 2018;373:95–102.

67. Skyllas-Kazacos M, Rychcik M, Robins RG, Fane AG, Green MA. New All-Vanadium Redox Flow Cell. J. Electrochem. Soc. 1986;133:1057.

68. Kim KJ, Lee SW, Yim T, Kim JG, Choi JW, Kim JH, et al. A new strategy for integrating abundant oxygen functional groups into carbon felt electrode for vanadium redox flow batteries. Sci Rep 2014;4:6906.

69. Ma K, Zhang Y, Liu L, Xi J, Qiu X, Guan T, et al. In situ mapping of activity distribution and oxygen evolution reaction in vanadium flow batteries. Nat Commun 2019;10:5286.

70. Cheng Y, Wang X, Huang S, Samarakoon W, Xi S, Ji Y, et al. Redox Targeting-Based Vanadium Redox-Flow Battery. ACS Energy Lett. 2019;4:3028–35.

71. Electrochemical Methods: Fundamentals and Applications, 3rd Edition | Wiley [Internet]. Wiley.com [cited 2024 Apr 29];Available from: https://www.wiley.com/en-us/Electrochemical+Methods%3A+Fundamentals+and+Applications%2C+3rd+Edition-p-9781119334057

72. Electrochemical Systems, 4th Edition | Wiley [Internet]. Wiley.com [cited 2024 May 9];Available from: https://www.wiley.com/en-us/Electrochemical+Systems%2C+4th+Edition-p-9781119514602

73. Zhang F, Liu J, Yang W, E. Logan B. A thermally regenerative ammonia-based battery for efficient harvesting of low-grade thermal energy as electrical power. Energy & Environmental Science 2015;8:343–9.

74. Kim KJ, Kim YJ, Kim JH, Park MS. The effects of surface modification on carbon felt electrodes for use in vanadium redox flow batteries. Materials Chemistry and Physics 2011;131:547–53.

75. Kimura C, Yamamuro Y, Aoki H, Sugino T. Improved field emission characteristics of carbon nanofiber treated with nitrogen plasma. Diamond and Related Materials 2007;16:1383–7.

76. Xie H, Jiang W, Liu T, Wu Y, Wang Y, Chen B, et al. Low-Energy Electrochemical Carbon Dioxide Capture Based on a Biological Redox Proton Carrier. Cell Reports Physical Science 2020;1:100046.

77. Wang M, Hariharan S, Shaw RA, Hatton TA. Energetics of electrochemically mediated amine regeneration process for flue gas CO2 capture. International Journal of Greenhouse Gas Control 2019;82:48–58.

78. Voskian S, Alan Hatton T. Faradaic electro-swing reactive adsorption for CO 2 capture. Energy & Environmental Science 2019;12:3530–47.

79. Liu Y, Ye HZ, Diederichsen KM, Van Voorhis T, Hatton TA. Electrochemically mediated carbon dioxide separation with quinone chemistry in salt-concentrated aqueous media. Nat Commun 2020;11:2278.